Available online at www.sciencedirect.com
ScienceDirect
Journal of the European Ceramic Society 28 (2008) 2463–2469
www.elsevier.com/locate/jeurceramsoc

Influence of macroscopic residual stresses on the mechanical behavior and microstructure of porcelain tile☆

Agenor De Noni Jr.[a,*], Dachamir Hotza[b], Vicente Cantavella Soler[c], Enrique Sanchez Vilches[c]

[a] *Instituto Maximiliano Gaidzinski (IMG), 88845-000 Cocal do Sul, SC, Brazil*
[b] *Universidade Federal de Santa Catarina (UFSC), 88040-900 Florianópolis, SC, Brazil*
[c] *Instituto de Tecnologia Cerámica (ITC), 12006 Castellón, Spain*

Received 5 September 2007; received in revised form 29 February 2008; accepted 6 March 2008
Available online 28 April 2008

Abstract

The development of macroscopic residual stress, as in glass-tempering processes, was studied for porcelain tile. Mechanical strength was observed to increase less than might be theoretically expected, owing to deterioration of the sintered tile microstructure. A model has been developed, using linear elastic fracture mechanics, to estimate the natural flaw size in the tempered material. The study shows that as the cooling rate raises, the macroscopic residual stress and flaw size increase. This microstructural deterioration is mainly attributed to the allotropic transformation of quartz in the presence of thermal tensile stress at the porcelain tile surface.

Keywords: Firing; Defects; Mechanical properties; Porcelain; Traditional ceramics; Tiles

1. Introduction

1.1. Porcelain tile

Porcelain tile, which is characterized by a large quantity of glassy phase and low porosity, has excellent technical and aesthetic properties. The tile is basically made from clays, kaolins, feldspars, and quartz. Clays and kaolins provide plasticity and dry mechanical strength and form mullite and glassy phase during firing; feldspars are low-temperature glassy phase formers; and quartz contributes to thermal and dimensional stability, because it is the most refractory constituent.[1]

Porcelain tile compositions are formulated and processed to allow a rapid firing cycle of 40–60 min. The peak firing temperature, between 1180 and 1220 °C, is typically determined by establishing the temperature at which maximum densification is reached. Following densification, water absorption is less than 0.5% and closed porosity lies between 3 and 7%. Cooling is carried out as rapidly as possible in industrial practice, with little control over the variables of this firing cycle stage. Only the allotropic transformation temperature of quartz (573 °C) is taken into account by reducing the cooling rate to avoid tile breakage. Rapid cooling then immediately continues again and is maintained until the tile leaves the kiln.[1]

1.2. Mechanical properties of porcelain materials

There are basically three theories that explain the strengthening mechanism in triaxial porcelains,[2] which may be applied to porcelain tiles:[3] interconnection of acicular mullite crystals; dispersion of crystalline phases that limit the natural flaw size; and matrix strengthening as a result of the difference between the linear thermal expansion coefficients of the matrix and those of the disperse crystalline phases. These mechanisms act simultaneously, making it difficult to determine categorically which one contributes most.

In addition, the level of complexity of this system is further increased because porcelain tile may develop a macroscopic residual stress profile[4] resembling that typically found in glass-tempering processes.[5,6] This occurs as a result of the rapid

☆ Based in part on the thesis submitted by A. De Noni Jr. for the Ph.D. degree in Materials Science and Engineering (PGMAT), Universidade Federal de Santa Catarina (UFSC), Brazil, 2007.

* Corresponding author. Tel.: +55 48 3441 7736; fax: +55 48 3441 7736.
E-mail address: agenor@imgnet.org.br (A. De Noni Jr.).

0955-2219/$ – see front matter © 2008 Elsevier Ltd. All rights reserved.
doi:10.1016/j.jeurceramsoc.2008.03.003

cooling rate in industrial firing cycles and the large quantity of glassy phase (50–65%) that develops during firing in porcelain tile, as in other types of ceramic materials.[7–9]

A significant difference with respect to traditional glass tempering is that the quartz particles (which are not present in glass) give rise to peripheral cracks in the interfaces with the matrix to provide microscopic stress relaxation.[2] During rapid cooling, thermal tensile stresses develop at the surface. For this reason, starting at the allotropic transformation temperature of quartz, subcritical growth of peripheral cracks may lead to microstructural deterioration, which will severely affect the tile mechanical behavior.

This study analyses how the cooling stage of the firing cycle influences porcelain tile microstructure and mechanical behavior. A model has been developed for this purpose, based on linear elastic fracture mechanics, which allows estimation of the effect of the cooling rate on the variation of the natural flaw size in the material. The results have been corroborated by scanning electron microscopy (SEM) observation of the microstructures of some of the pieces obtained.

2. Mathematical modeling

2.1. Basic concepts

In accordance with linear elastic fracture mechanics, the mechanical strength of a material, σ_f, is given by the following equation[10]:

$$\sigma_f = \frac{K_{Ic}}{Ya^{1/2}} \tag{1}$$

where K_{Ic} is the fracture toughness; a, the natural flaw size; and Y, the calibration factor.

The presence of a macroscopic stress profile inside the piece will lead to a modification of toughness. The fracture toughness (K_r) associated with a residual stress profile throughout the thickness of the material $\sigma_r(x)$ is expressed by the following equation[10,11]:

$$K_r = \frac{Y}{\pi a^{1/2}} \int_0^a \sigma_r(x) g(x)\, dx \tag{2}$$

where $g(x)$ is the Green's function, which is dependent on the particular configuration of the stress application and crack propagation system. For the system described in Fig. 1, $g(x) = 2a/(a^2 - x^2)^{1/2}$, and $Y = 1.985$.

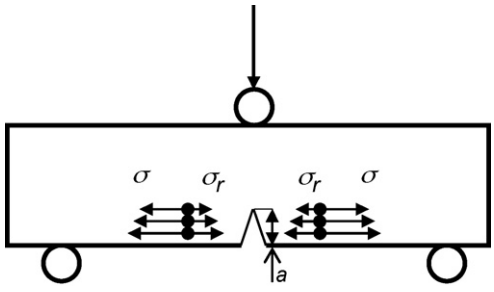

Fig. 1. Fracture propagation under a bending stress (adapted from Ref. 11).

The apparent toughness of a material with a macroscopic stress profile ($\bar{K}_{Ic}$) may be expressed by the following equation[11]:

$$\bar{K}_{Ic} = K_{Ic} - K_r \tag{3}$$

Thus, compressive residual stress raises apparent toughness, since K_r is negative. For typical tempering stress profiles, apparent toughness maximizes at the surface and decreases progressively inwards into the material. This can lead to unstable crack growth and subsequent catastrophic fracture of the material. However, these concepts are used to develop functional gradients in tempered glasses in order to produce stable fracture growth regions.[12,13]

2.2. Estimate of bending strength after tempering of porcelain tile

The mechanical strength of a material with a macroscopic residual stress profile may also be written as

$$\sigma_{ta} = \frac{\bar{K}_{Ic}}{Ya^{1/2}} \tag{4}$$

Combining Eqs. (3) and (4) gives:

$$\sigma_{ta} = \frac{K_{Ic}}{Ya^{1/2}} - \frac{K_r}{Ya^{1/2}} \tag{5}$$

If Eq. (2) is substituted for K_r it is necessary to consider a given residual stress profile in order to solve the integral. The residual stress profile may be considered as approximately proportional to the second-degree Legendre polynomial[14]:

$$\sigma_r(x') = \sigma_s(6x'^2 - 6x' + 1) \tag{6}$$

where σ_s is the residual stress at the surface; and $0 \le x' \le 1$, the domain of the function.

For small thickness values, $0 \le x' \le a$, x'^2 assumes such small values that these may be considered negligible compared with x'. Hence, in a plane near the surface, residual stress may be

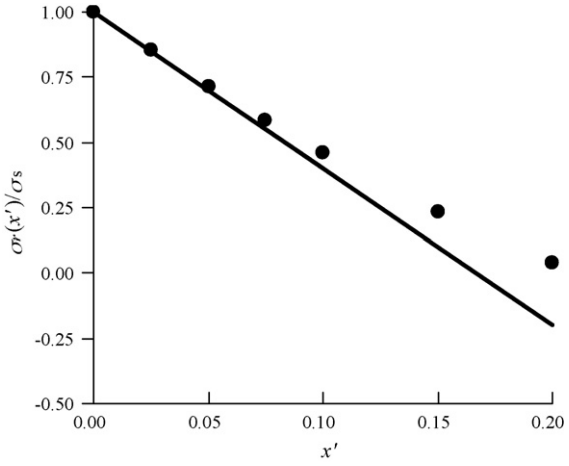

Fig. 2. Graphic representation of the linearization of the residual stress profile near the surface.

expressed by a linear equation (Eq. (7)). Fig. 2 is a graphic representation of this linearization:

$$\sigma_r(x') = \sigma_s(-6x' + 1) \quad (7)$$

Writing Eq. (7) for the test piece thickness (h) domain gives:

$$\sigma_r(x) = \sigma_s(Sx + 1) \quad (8)$$

$$S = \frac{-6}{h} \quad (9)$$

Substituting Eq. (8) in Eq. (2), the integral presents the analytical solution expressed by the following equation:

$$K_r = \frac{Y}{\pi a^{1/2}}\sigma_s(2Sa^2 + \pi a) \quad (10)$$

The equation that predicts the mechanical strength of a material with macroscopic residual stress, Eq. (5), may thus be written as follows:

$$\sigma_{ta} = \frac{K_{Ic}}{Ya^{1/2}} - \sigma_s\left(\frac{2S}{\pi}a + 1\right) \quad (11)$$

All the parameters in Eq. (11), except natural flaw size (a), can be determined experimentally. The value of 'a' can be calculated by iterative methods.

In a limit case, where there is no macroscopic residual stress at the surface ($\sigma_s = 0$), Eq. (11) becomes the classic linear elastic fracture mechanics equation, Eq. (1). Another limit situation is that in which the following assumptions are met: (A) natural flaw size in the product with residual stresses is equal to that in the residual stress-free product, $a = a_0$; (B) compressive stress near the surface is constant at least throughout a thickness equivalent to the size of the flaw, $S = 0$ for $0 \le x \le a$. Eq. (11) them adopts its simplest form[13,15]

$$\sigma_{ta} = \sigma_o - \sigma_s \quad (12)$$

where σ_o is the mechanical strength of slow-cooled material.

However, in the case of porcelain tile these assumptions may not be met, chiefly because the natural flaw size of the tempered product may be larger than that of the residual stress-free product, as a result of the microstructural deterioration indicated in Section 1.2. Fig. 3 illustrates this situation. In this figure, σ_o^* represents the mechanical strength of the residual stress-free material, but with the same size of natural flaw as in the tempered material.

Once the flaw size is calculated according to Eq. (11), one can calculate the apparent toughness through Eq. (4).

3. Experimental procedure

3.1. Preparation of test pieces

Test pieces of 80 mm × 20 mm × 7 mm were pressed from an industrial spray-dried powder used in porcelain tile manufacture composed (weight basis) of: 35% clay and kaolin; 55% potash and sodium feldspar; 6% quartz; 4% talc. The powder had a 5.5% moisture content (dry weight basis), and a compacting pressure of 45 MPa was used. After drying in an oven at 110 °C, the test

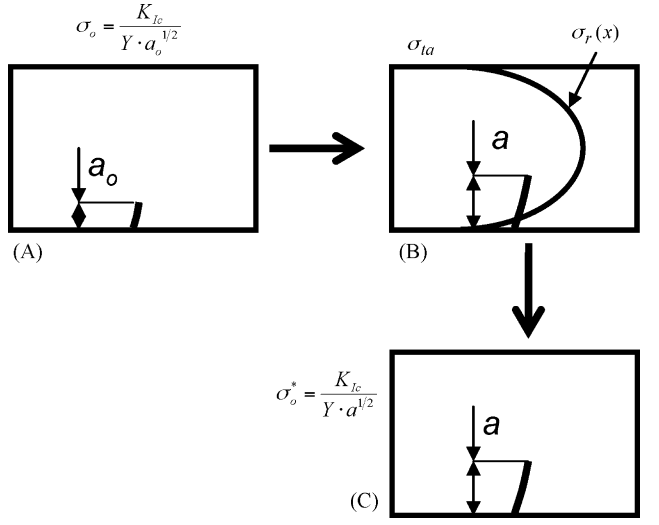

Fig. 3. Apparent mechanical strength of the material in different configurations: (A) material with natural microstructural deterioration, without residual stresses; (B) material with increased microstructural deterioration and residual stresses; (C) material with increased microstructural deterioration, without residual stresses.

pieces were fired in an electric kiln (Pirometrol model R). The heating rate was 70 °C/min from 25 to 500 °C, and 25 °C/min from 500 to 1190 °C in every firing. The hold time at peak firing temperature (1190 °C) was 6 min; this peak temperature was chosen because the product achieved maximum densification at this temperature in the tested firing cycle. Six different cooling modes were used, which are described below.

3.2. Cooling modes used

The different cooling modes are referenced E1 to E6. In these experiments the cooling rate was mainly modified in the temperature range in which the glassy matrix is predominantly viscoelastic, i.e. from peak firing temperature (1190 °C) to approximately 650 °C (the glass transition temperatures of natural orthoclase and albite glasses are 875 and 815 °C, respectively[16]), and in the temperature range in which the glassy matrix is elastic ($T < 650$ °C) and the allotropic transformation of quartz occurs. The following sequence lists, in ascending order, the tested cooling modes according to their degree of severity regarding both the generation of macroscopic stresses and the microstructural deterioration associated with quartz transformation:

E1 < E2 < E3 < E4 < E5 < E6

E1 cooling corresponds to natural cooling in the kiln. E2 cooling also took place in the kiln, in this case using the kiln ventilation system. The other coolings took place outside the kiln using the setup shown in Fig. 4.

The refractory grid with eight test pieces (P1) was withdrawn from the kiln at peak firing temperature and placed on a refractory support (P2) equipped with two fans (P3: Jata model 38) and a compressed-air distribution system (P4). The compressed-air system consisted of a 12 mm copper tube in which a row of 1 mm holes spaced every 2.5 mm had been drilled. The tube was

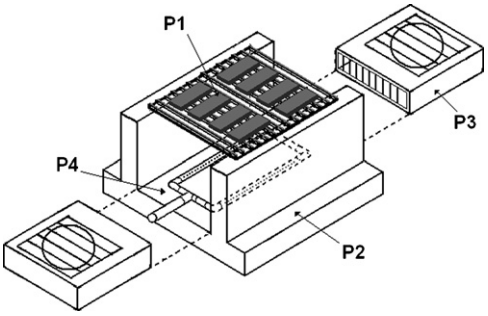

Fig. 4. Setup used for rapid cooling outside the kiln, comprising a refractory grid and test pieces (P1), a refractory support (P2), two side fans (P3), and a compressed-air distributor (P4).

Table 1
Cooling rates used to obtain the test pieces

	Cooling rate (°C/s)		
	850–650 °C	650–500 °C	Mean
E1	0.1	0.1	0.1
E2	0.7	0.6	0.6
E3	3.4	3.0	3.2
E4	4.7	3.2	4.0
E5	9.5	3.6	6.6
E6	9.5	7.6	8.6

bent to form a 120 mm × 80 mm rectangle, as shown in Fig. 4, and was connected to an air-pressure circuit operating at 6 bar. The distance between the copper tube and the specimens was 100 mm.

E3 cooling was achieved by natural convection without using the forced convection system, while in E4 the fans were turned on during the first cooling stretch (to ~650 °C). E5 and E6 were carried out with the fans and compressed air; however, in E5 forced convection was only applied to ~650 °C, while in E6, forced convection was applied throughout the entire cooling period. Table 1 presents the cooling rates obtained with this setup, measured using a thermal infrared camera (ThermalCam E/B2 from Flir Systems) with special lenses for temperatures up to 900 °C. It may be noted by comparison that industrial cooling is close to E4.

3.3. Properties measured

The mean mechanical strength was determined by three-point bending tests with 12 samples for each cooling condition using a universal testing machine (Instron 6027). The error bars were determined using the *t*-Student's distribution ($t_{0.05} = 1.795$).

Residual stresses were measured in a test piece from each type of cooling by the deformation–relaxation method with incremental cuts,[5] using a 0.4-mm-thick diamond cutting disc and rectangular strain gauges with a 3-mm-long grid (HBM). The method is based on making a slot (or crack) of depth a_i in the specimen. This produces a deformation (Fig. 5) which is measured using a strain gauge. As the slot depth increases, the strain changes, from which the original stress profile may be reconstructed.

To carry out the stress profile calculation it is useful to express the free strain profile as a linear combination of Legendre polynomials (P_k):

$$\varepsilon_f = \sum_{k=0}^{n_P-1} \varepsilon_{f,k} = \sum_{k=0}^{n_P-1} \lambda_k P_k(\zeta) \tag{13}$$

where n_P is the number of Legendre polynomials used in the expansion, λ_k are the Legrendre coefficients (unknowns) and ζ is the adimensional coordinate along the depth ($\zeta = -1$: bottom surface; $\zeta = +1$: top surface).

Once λ_k has been calculated, it is possible to evaluate the residual stresses from equation:

$$\frac{\sigma_r(\zeta)}{E} = -\sum_{k=2}^{n_P} \lambda_k P_k(\zeta) \tag{14}$$

Fracture toughness (K_{Ic}) of the residual stress-free material (E1 cooling), determined by the single-edge-notched beam (SENB) method (10 samples), was 1.55 ± 0.04 MPa m$^{1/2}$. Values between 1.3 and 2.0 MPa m$^{1/2}$ are common in the literature for porcelain tile[17,18] and also for triaxial porcelain[19,20]. However, values between 1.5 and 1.8 MPa m$^{1/2}$ are so normal according to composition, particle size, processing and test method applied in this work.

The test pieces obtained by E1 and E5 cooling were examined by SEM (Philips model XL30 CP), observing cross-sections of the microstructure near the surface.

4. Results and discussion

4.1. Surface residual stress

The surface residual stress resulting from the tempering process is plotted versus cooling rate from 850 to 650 °C in Fig. 6. Typical linear behavior may be observed,[6] in which residual stress increases as the material cools more rapidly in the temperature range in which the tempering process occurs. The point corresponding to E6 cooling displays a residual stress value below the expected trend. In this particular case, the test pieces broke during the residual stress test at notch depths close to 1/3 of the piece thickness as a result of the severe microstructural deterioration the pieces had suffered under these cooling conditions. The resulting value therefore displays a larger experimental error than the other points. It must be remembered that forced con-

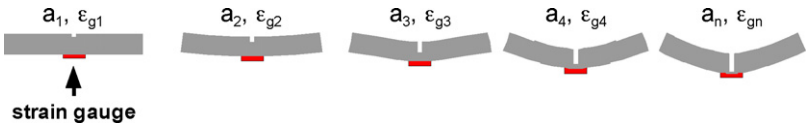

Fig. 5. Foundations of the strain relaxation slotting method.

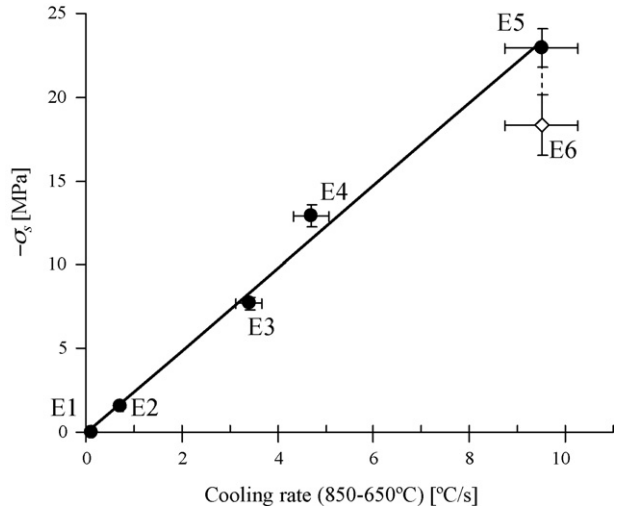

Fig. 6. Surface residual stress vs. the cooling rate from 850 to 650 °C.

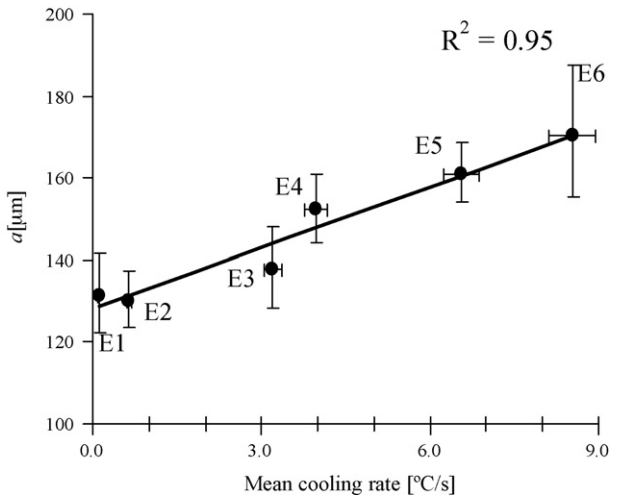

Fig. 8. Natural flaw size (a), calculated from Eq. (11), vs. the mean cooling rate.

vection was applied throughout E6 cooling, even during the allotropic transformation of quartz.

4.2. Bending strength

Mechanical strength (σ_{ta}) is plotted versus surface residual stress ($-\sigma_s$) in Fig. 7. Since the stress is compressive, an increase in mechanical strength is found in every case. The straight line corresponds to the theoretical value calculated from Eq. (11), assuming that natural flaw size does not change with residual stresses ($a = a_0$). The discrepancy exhibited by the experimental data from the theoretical results is related to the microstructural deterioration that occurs in the test pieces as a result of the microscopic stress relaxation induced by the quartz particles.[4] This microstructural deterioration worsens as cooling becomes more severe, especially during the allotropic transformation of quartz. Fig. 7 also shows the apparent toughness ($\bar{K}_{Ic}$) as a function of macroscopic residual stress. It can be observed that apparent toughness increases in proportion to the residual stress increase, so the tempering in porcelain tile can be considered a toughening mechanism.

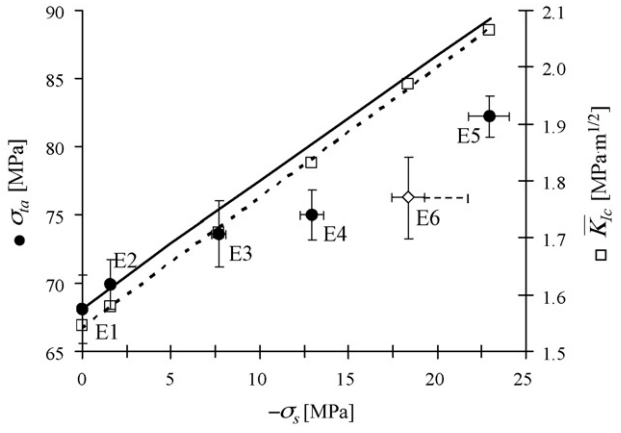

Fig. 7. Mechanical strength (σ_{ta}) vs. surface residual stress ($-\sigma_s$); the straight line corresponds to the theoretical value deduced from Eq. (11), for $a = a_0$.

4.3. Estimation of natural flaw size

Natural flaw size (a), calculated from Eq. (11), is plotted versus the mean of the cooling rates detailed in Table 1 and Fig. 8. The flaw size of the residual stress-free material resulting from the slowest cooling (E1) was about 130 µm. Typical values reported by other authors[3,17,18] range from 100 to 200 µm. It may be observed that natural flaw size increases as the cooling rate rises. The figure also shows that no test piece displayed a smaller flaw than that of the slowly cooled material; this result is a necessary condition for the validation of the mathematical model used. On the other hand, the cooling rate up to 3.2 °C/s (E3) does not significantly change the flaw size. Up to this point the instantaneous tensile stress during cooling is probably less than the stress needed to produce a subcritical increase in flaw size.

Microstructural flaws in porcelain tile chiefly originate after the glass transformation temperature of the matrix. Although the disperse crystalline particles may limit natural flaw size growth,[21] the quartz particles detaching from the matrix can have the opposite effect, mainly for particles larger than about 50 µm.[22,23] In addition, the presence of instantaneous surface tensile stresses, especially after the allotropic transformation of quartz, is a favorable condition for an increase in natural flaw size during the cooling stage. The faster the cooling from 650 to 500 °C, the greater the magnitude of these stresses will be. The thermal gradients needed to develop macroscopic residual stresses between 850 and 650 °C remain significant during the allotropic transformation of quartz. Thus, the mean cooling rate of these two temperature ranges represents, indirectly, the magnitude of the thermal tensile stresses at the surface.

4.4. Microstructural analysis

Microscopic observation of crack growth is very complex because the polishing operation for sample preparation also causes microstructural deterioration. However, two materials with different states of initial deterioration, subjected to the same

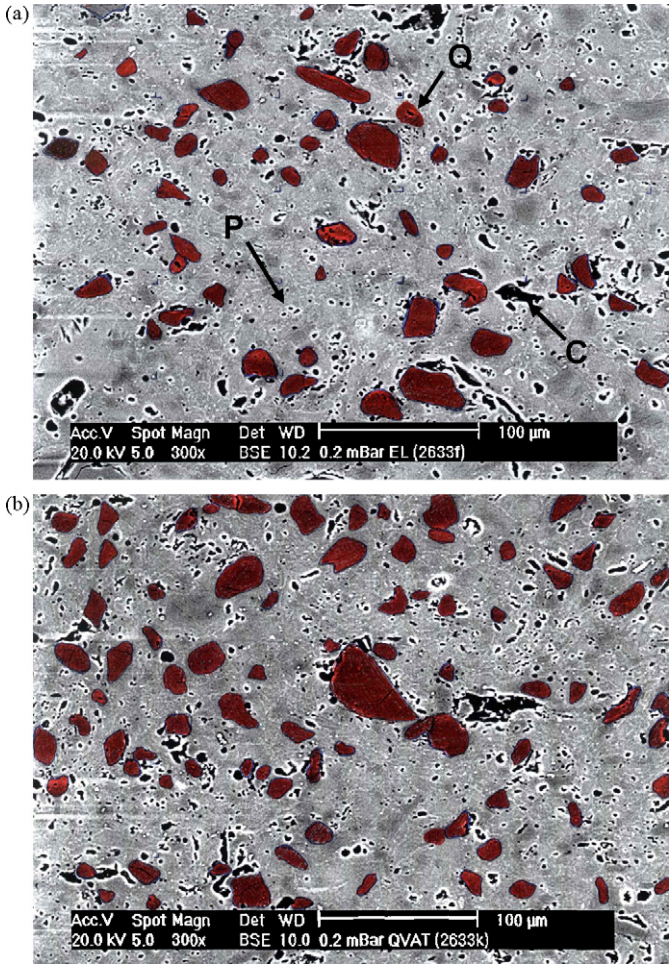

Fig. 9. Microstructural regions quantified by image analysis. (Q) Quartz particles, (P) porosity, (C) chipping. (a) E1 slow cooling and (b) E5 rapid cooling. Magnification 300×.

polishing conditions, may be expected to display different states of microstructural deterioration.

It has been possible to differentiate two extreme cases (E1 and E5) by inspecting a 12×10^4 μm^2 surface area of each test piece at a magnification of 300× in the scanning electron microscope (Philips XL30 CP), shown in Fig. 9. This allowed identification of the quartz particles (Q) that had given rise to cracks in the matrix (darker regions in the images in Fig. 9). The area occupied by these particles (referenced $A - \mathrm{QMC}$) was then calculated. Mean quartz particle size (D_{50}) and the area occupied by porosity + chipping (AP + AC) were also calculated. The results are shown in Table 2.

Table 2
Image analysis results of test pieces obtained by E1 slow cooling and E5 rapid cooling

Property	E1 (slow) Fig. 8	E5 (rapid) Fig. 8
AP + AC (%)	6.2	6.5
$A - \mathrm{QMC}$ (%)	8.4	15.3
D_{50} (μm)	13.1	13.7

Both cases display similar characteristics for the area occupied by porosity (P) + chipping (C) as well as for the size of the quartz particles that had produced cracks in the matrix. However, in the case of the rapidly cooled piece, E5, the area occupied by the quartz particles with cracks in the matrix was almost twice that of the slowly cooled piece (E1). These results confirm that as the cooling rate rises, crack size increases more readily, encouraged by thermal stresses, leading to more severe microstructural deterioration.

5. Conclusions

Porcelain tile mechanical strength increases as a result of macroscopic residual stresses that develop during rapid cooling in the firing cycle, just as in glass tempering. It can be considered a toughening mechanism. However, this increase is less than might be expected, owing to the microstructural deterioration produced in the material. This deterioration is due to subcritical growth of the cracks that form in the material (a contributory factor also being the deterioration caused by the quartz particles with the largest diameters) in the presence of thermal tensile stresses at the surface during cooling.

A model has been developed, based on linear elastic fracture mechanics, which allows estimation of the increase in natural flaw size. Image analysis shows that microstructural deterioration worsens as the cooling rate increases. The model also confirms that the greatest microstructural deterioration is related to a larger natural flaw size, as a result of subcritical growth of the microcracks.

The possibility of estimating the variation in natural flaw size after porcelain tile cooling is of particular interest for the comparative study of the behavior of different raw materials compositions subjected to the same cooling conditions. This might allow new mixtures to be formulated for optimizing the firing process and product end properties.

Acknowledgements

The authors wish to thank the staff at the Instituto de Tecnología Cerámica (ITC), Spain, the staff at Maximiliano Gaidzinski Institute (IMG), Brazil. This work was financially supported by the Brazilian Research Agency CAPES, under scholarship 2933-05-5 and the Spanish Ministry of Industry, Tourism, and Trade for co-financing the Technology Institute Support Programme (FIT-030000-2005-315/FIT-030000-2006-119).

References

1. Sánchez, E., Orts, M. J., Ten, J. G. and Cantavella, V., Porcelain tile composition: effect on phase formation and end products. *Am. Ceram. Soc. Bull.*, 2001, **80**, 43–49.
2. Carty, W. M. and Senapati, U., Porcelain—raw materials, processing, phase evolution, and mechanical behavior. *J. Am. Ceram. Soc.*, 1998, **81**, 3–20.
3. Cavalcante, P. M. T., Dondi, M., Ercolani, G., Guarini, G., Melandri, C., Raimondo, M. and Almendra, E. R., The influence of microstructure on the performance of white porcelain stoneware. *Ceram. Int.*, 2004, **30**, 953–963.

4. De Noni Jr., A. *Estudo das Propriedades Mecânicas de Porcelanato Através da Avaliação de Tensões Residuais Microscópicas e Macroscópicas Originadas Durante a Etapa de Resfriamento do Ciclo de Queima*, PhD thesis, Universidade Federal de Santa Catarina, Florianópolis, SC, Brazil, 2007.
5. McMaster, R. A., Fundamentals of tempered glass. *Ceram. Eng. Sci. Proc.*, 1989, **10**, 193–206.
6. Navarro, J. M. F. and Vidrio, El. *Constitución, Fabricación y Propiedades* (*The Glass: Constitution, Processing and Properties*), CSIC, Madrid, 2003.
7. Ohira, H. and Bradt, R. C., Strength distributions of a quench-strengthened aluminosilicate ceramic. *J. Am. Ceram. Soc.*, 1988, **71**, 35–41.
8. Insley, R. H. and Barczak, V. J., Thermal conditioning of polycrystalline alumina ceramics. *J. Am. Ceram. Soc.*, 1964, **47**, 1–4.
9. Gruver, R. M. and Kirchner, H. P., Residual stress and flexural strength of thermally conditioned 96% alumina rods. *J. Am. Ceram. Soc.*, 1968, **51**, 232–233.
10. Green, D. J., *Introduction to Mechanical Properties of Ceramics*. Cambridge University Press, Cambridge, 1998.
11. Sglavo, V. M., Larentis, L. and Green, D. J., Flaw-insensitive ion-exchanged glass. I. Theoretical aspects. *J. Am. Ceram. Soc.*, 2001, **84**, 1827–1831.
12. Sglavo, V. M. and Green, D. J., Flaw-insensitive ion-exchanged glass. II. Production and mechanical performance. *J. Am. Ceram. Soc.*, 2001, **84**, 1832–1838.
13. Sglavo, V. M., Prezzi, A. and Alessandrini, M., Processing glasses with engineered stress profiles. *J. Non-Cryst. Sol.*, 2004, **344**, 73–78.
14. Arfken, G. B. and Weber, H. J., *Mathematical Methods for Physicists*. Elsevier Academic Press, Burlington, 2005.
15. Lu, J., *Handbook of Measurement of Residual Stress*. Fairmont Press, Lilburn, 1996.
16. Vergano, P. J., Hill, D. C. and Uhlmann, D. R., Thermal expansion of feldspar glasses. *J. Am. Ceram. Soc.*, 1967, **50**, 59–60.
17. Tucci, A., Esposito, L., Malmusi, L. and Rambaldi, E., New body mixes for porcelain stoneware tiles with improved mechanical characteristics. *J. Eur. Ceram. Soc*, 2007, **27**, 1875–1881.
18. Carbajal, L., Rubio-Marcos, F., Bengochea, M. A. and Fernandez, J. F., Properties related phase evolution in porcelain ceramics. *J. Eur. Ceram. Soc.*, 2007, **27**, 4065–4069.
19. Bragança, S. R., Bergmann, C. P. and Hübner, H., Effect of quartz particle size on the strength of triaxial porcelain. *J. Eur. Ceram. Soc.*, 2006, **26**, 3761–3768.
20. Maity, S. and Sarkar, B. K., Development of high-strength whiteware bodies. *J. Eur. Ceram. Soc.*, 1996, **16**, 1083–1088.
21. Borom, M. P., Dispersion-strengthened glass matrices-glass-ceramics, a case in point. *J. Am. Ceram. Soc.*, 1977, **60**, 17–21.
22. Warshaw, S. I. and Seider, R. J., Comparison of strength of triaxial porcelains containing alumina and silica. *J. Am. Ceram. Soc.*, 1967, **50**, 337–342.
23. Bragança, S. R. and Bergmann, C. P., A view of whitewares mechanical strength and microstructure. *Ceram. Int.*, 2003, **29**, 801–806.